Geotechnical and Geological Engineering (2006) 24: 1581–1602
DOI 10.1007/s10706-005-3811-1

Mapping the liquefaction induced soil moisture changes using remote sensing technique: an attempt to map the earthquake induced liquefaction around Bhuj, Gujarat, India

D. RAMAKRISHNAN[1,★], K.K. MOHANTY[2], S.R. NAYAK[2]
and R. VINU CHANDRAN[3]
[1]*Department of Earth Sciences, Indian Institute of Technology, Powai, Mumbai 400 076, India*
[2]*MWRG, Space Applications Centre, Ahmedabad 380 015, India*
[3]*RRSSC-ISRO, IIT Campus, Kharagpur 721 302, India*

(Received 8 July 2004; accepted 6 October 2005)

Abstract. The Bhuj earthquake (Mw = 7.9) occurred in the western part of India on 26th January 2001 and resulted in the loss of 20,000 lives and caused extensive damage to property. Soil liquefaction related ground failures such as lateral spreading caused significant damage to bridges, dams and other civil engineering structures in entire Kachchh peninsula. The Bhuj area is a part of large sedimentary basin filled with Jurassic, Tertiary and Quaternary deposits. This work pertains to mapping the areas that showed sudden increase in soil moisture after the seismic event, using remote sensing technique. Multi-spectral, spatial and temporal data sets from Indian Remote Sensing Satellite are used to derive the Liquefaction Sensitivity Index (LSeI). The basic concept behind LSeI is that the near infrared and shortwave infrared regions of electromagnetic spectrum are highly absorbed by soil moisture. Thus, the LSeI is herein used to identify the areas with increase in soil moisture after the seismic event. The LSeI map of Bhuj is then correlated with field-based observation on Cyclic Stress Ratio (CSR) and Cyclic Resistance Ratio (CRR), depth to water table, soil density and Liquefaction Severity Index (LSI). The derived LSeI values are in agreement with liquefaction susceptible criteria and observed LSI ($R^2 = 0.97$). The results of the study indicate that the LSeI after calibration with LSI can be used as a quick tool to map the liquefied areas. On the basis of LSeI, LSI, CRR, CSR and saturation, the unconsolidated sediments of the Bhuj area are classified into three susceptibility classes.

Key words. Gujarat earthquake 2001, liquefaction sensitivity index, liquefaction severity index, remote sensing.

1. Introduction

On 26th January 2001, when India was preparing to celebrate its 51st Republic Day, the most devastating earthquake (Mw 7.9 – USGS) of the recent history struck the Kachchh area of Gujarat. This strong intra-cratonic earthquakes in quick succession necessitated complete understanding of tectonics and revision of existing seismic zonation. The Bhuj area (Figure 1) has witnessed several hundreds of earthquakes

★ Corresponding author: e-mail: aarkay_geol@yahoo.com

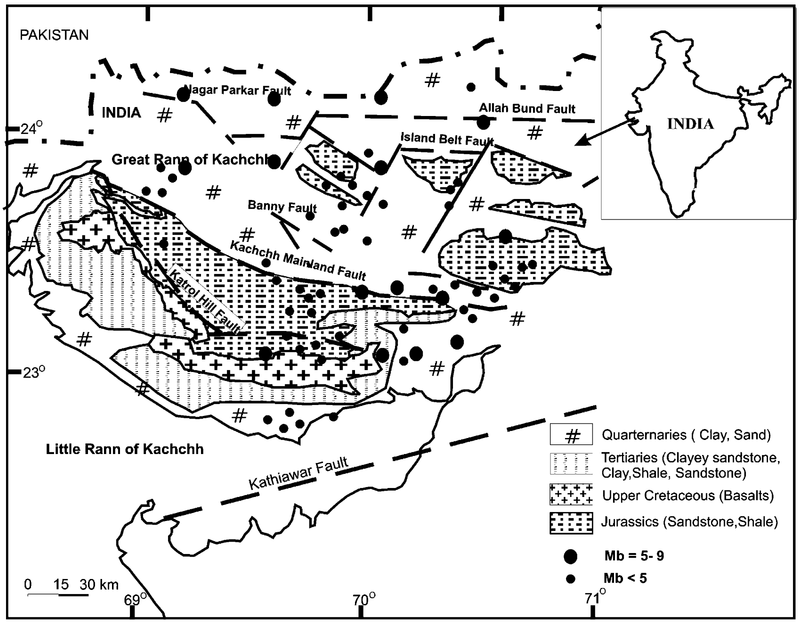

Figure 1. Regional Geology and Seismotectonic setup of Kachchh Peninsula, India.

from the historical period to this date (Malik et al., 1999). When the prediction of seismic event is still rudimentary, the developments in science and technology can at least be effectively utilized to minimize the deleterious effects of an earthquake. All the efforts to minimize the devastating effects of earthquake and associated events begin with the procedure of micro-seismic zonation (MSZ) and development of structural codes. The calamities of the recent earthquake made the scientific community in India (Iyengar and Raghukanth, 2002; Karanth et al., 2001; Rajendran et al., 2001; Jade et al., 2001) and abroad (Bilham, 2001; Krinitzsky and Hynes, 2002; Tuttle and Hengesh, 2002) to contribute from different angles converging towards MSZ. One among the important components of MSZ is mapping the liquefaction potential (LP) areas. It is not over emphasized to state that maximum devastation to structures is caused due to liquefaction related ground failures (Youd and Perkins, 1987; Youd and Keefer, 1981).

Application of remote sensing technique to map accurately various aspects of earthquake related phenomena such as liquefaction (Gupta et al., 1998; Mohanty et al., 2001; Ray et al., 2001; Singh et al., 2001), damage (Sharma et al., 2003), landslides (Saraf, 2000), are fairly well established. The methodologies adopted by these workers include image differencing (Mohanty et al., 2001, Singh et al., 2001) and picture colour transformation (Saraf et al., 2002). These methods help in mapping the liquefaction accurately. However, classification of liquefaction on the basis of severity is not possible using these methods.

Though the Kachchh area has witnessed several devastative earthquakes in the recent history (Malik et al., 1999) not much work has been done on MSZ in general

and liquefaction susceptibility in particular. This paper attempts to map the areas that underwent sudden increase in soil moisture immediately after the Bhuj earthquake in 2001 using the onboard scanners of Indian Remote Sensing Satellite (IRS-1C). Subsequently, this map is correlated with filed based liquefaction susceptibility criteria (CRR, CSR) and liquefaction severity to arrive at meaningful conclusion.

2. Geology and Seismo-tectonics of the Study Area

The Kachchh Peninsula forms the western most part of the Indian sub-continent. The mainland Kachchh is a peneplain and occupied by Rann of Kachchh sediments and volcanic basalts. The seismo-tectonic setup of Kachchh region (Figure 1) attracted the geologists, seismologist and archaeologists alike for almost a century (Oldham, 1926; Biswas and Khattari, 2002; Bilham, 2001; Sohani, 2002).

The Kachchh region comprises of mainly Mesozoic (sandstones, siltstones, shale, and limestone), Tertiary (poorly consolidated sandstone, siltstone, and clay) and Quaternary (sand and clay) sedimentary sequences.

The Kachchh seismo-tectonic belt extends approximately 250 km (East–West) and 150 km (North–South). It is flanked in the north by Nagar Parkar fault and in the south by Kathiawar fault. The area in between is traversed by several faults/fault systems. Salient among them are Katrol Hill Fault (KHF), Kachchh Mainland Fault (KMF), Banni Fault (BF), Island Belt Fault (IBF) and Allah Bund Fault (ABF).

The Kachchh peninsula has experienced several episodes of ground movements along these East–West trending fault systems (Malik et al., 1999). Manifestations of these movements are strewn in the landscape of this area as well as in the form of palaeo-seismic indicators (Rajendran et al., 2001).

3. Methodology

The basic concept behind the present investigation is that the near infrared (NIR) and shortwave infrared (SWIR) regions (0.7–3.0 μm) of electromagnetic spectrum are highly absorbed by soil moisture. Reflectance of bare soil in this region of electromagnetic spectrum is inversely related to the moisture saturation. These spectral bands along with other bands such as Blue (0.4–0.5 μm), Green (0.5–0.6 μm) and Red (0.6–0.7μm) on board spacecraft/aircraft are widely used to estimate soil moisture (Wang et al., 2004). In the present investigation the following sensors onboard Indian Remote Sensing Satellite (IRS-1C) is used for detecting the changes in soil moisture by way of band ratios.

- Wide Field Sensor (WiFS) comprises NIR and Red bands with a ground resolution of 188 m.
- Linear Imaging Self-scanning Sensor (LISS-III) comprises Green, Red, and NIR and SWIR bands with a spatial resolution of 23.5 m.
- Panchromatic (PAN) sensor in the visible region with a spatial resolution of 5.8 m.

3.1. IMAGE PROCESSING

Since the present technique involves deriving band ratios between pre- and post-event satellite data, both data need to be geometrically registered with sub pixel accuracy. For geometric correction, 60 ground control points (GCP) are used to register the images using a second-order polynomial equation. By this way, the root mean square error is minimized to 0.05. Since, multi temporal data are used for analysis; the atmospheric effects of pre- and post-event data need to be compensated. The atmospheric effects are corrected by normalizing the Digital Number (DN) values/grey levels of post-event image to pre-event image. Reflectance signature from relatively unchanging objects such as deep-water body, rock exposures and roads are chosen from both pre- and post-images. A scatter plot is made between same wavelength regions of pre- and post-images. From these scatter plots, suitable regression equations are derived for each bands. These regression equations are used to normalize the DN values of post-event data.

Band ratios between the bands in which the feature of interest shows least correlation are widely used to maximize the typical reflectance (class) and minimize the reflectance of other feature classes (Townshend and Justice, 1986; Tucker and Sellers, 1986). Further, band ratios reduce the effects due to differential illumination within the same scene/image. Ratios among different bands/combinations of bands have also been effectively used to map different thematic features such as soil moisture, water body, snow cover and water stress in plants (McFeeters, 1996). In the present investigation we derived a band ratio using the Green (B1), Red (B2), NIR (B3) and SWIR (B4) bands of pre-event image and the same wavelengths B1′, B2′, B3′ and B4′ of the post-event image.

The image processing (rectification, radiometric normalization) and image analyses (band ratios) are carried out using ERDAS-imagine (ver. 8.5) software. Field data on SPT, *in situ* density and soil properties are evaluated following the Indian Standard procedures (IS: 2131–1981). Normalization and corrections for the SPT values are carried out following the procedures of Youd et al. (2001). Generation of various vector layers such as geology, litholog, SPT, ground water table and overlay analysis of field and satellite derived results are carried out in Geographic Information System (GIS) environment using ARC/Info ver.9.0 software. The detailed procedure adopted is illustrated in the flowchart (Figure 2).

Given below is the three-tier approach followed:

(1) Since WiFS data has high temporal frequency, small scale (1:250,000 scale) mapping of dynamic soil moisture changes is done using the band ratios of immediate pre- and post-earthquake images. For this purpose, WiFS data sets acquired on 23rd, 26th, 29th January 2001 and 1st, 4th of February 2001 are used. Since the WiFS data of 26th January 2001 was acquired 90 minutes after the earthquake, the real time effect of liquefaction and soil moisture changes could be mapped well. Data sets on 1st, 4th February 2001 are used to monitor the impact of post-quake tremors on soil moisture changes.

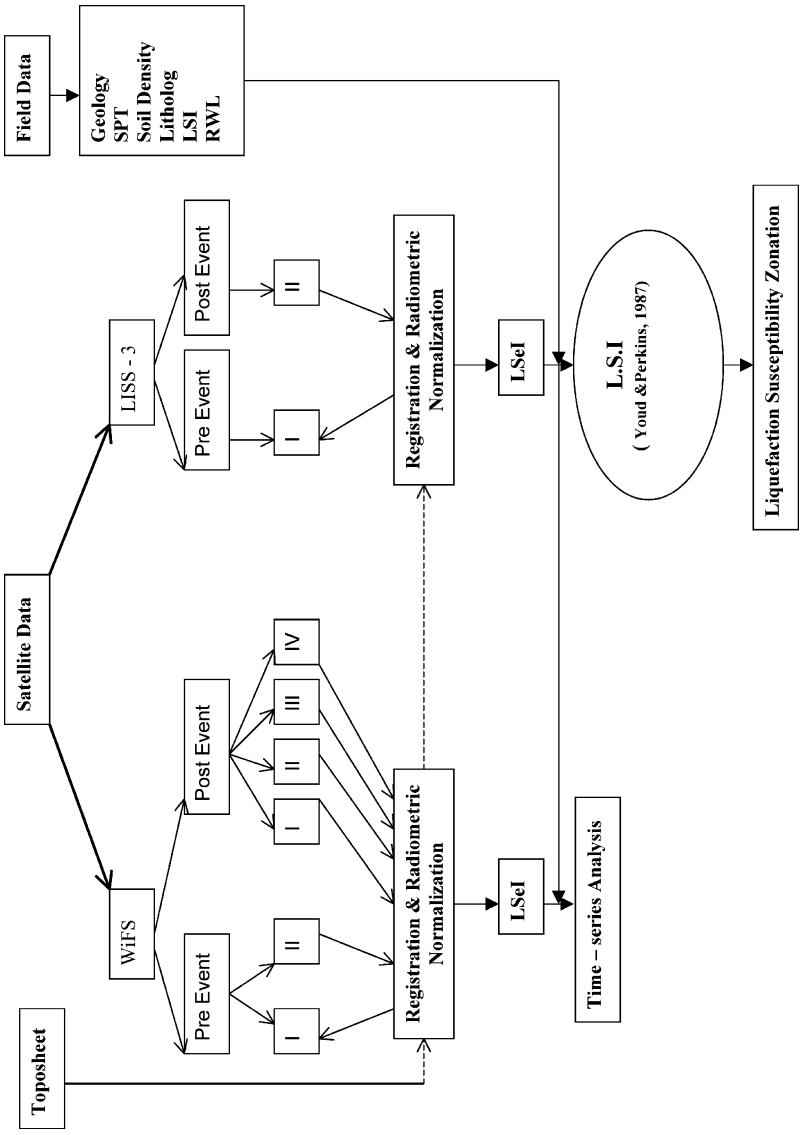

Figure 2. Schematic representation of the adopted methodology.

(2) Band ratios derived from LISS-III merged with PAN data sets of 4th (pre-event) and 29th (post-event) January 2001 are used to map liquefaction induced soil moisture changes on large scale (1:12,000). For this, the LISS-III image was transformed from Red, Green and Blue (RGB) domain to Intensity, Hue and Saturation (IHS) domain. Then the intensity component is replaced with the PAN data following the procedure given by Carper et al. (1990). This spatially enhanced map is used for LSeI estimation and further correlation with field data on liquefaction susceptibility.
(3) Third step is the generation of database in GIS environment on liquefaction susceptibility criteria such as geological map, SPT, density, depth to groundwater and estimation of liquefaction severity through Liquefaction Severity Index (LSI).

4. Results

4.1. LIQUEFACTION SENSITIVITY INDEX

Satellite sensors measure radiant energy of the objects on the ground. Water has high absorbance in the NIR and SWIR wavelengths. Hence, these bands are highly sensitive to changes in soil moisture. Attempts are herein made to arrive at a band ratio or combinations of band ratios that can detect change in soil moisture. Nine different ratios are attempted from simple differencing to combinations (Table 1). The images thus derived are correlated with field data on cyclic stress ratio (CSR) and cyclic resistance ratio (CRR) and LSI. Of the several band ratios attempted, the one given below is observed to correlate well with the field based liquefaction criteria.

$$\mathrm{LSeI} = [(\mathrm{B4}-\mathrm{B1}) * (\mathrm{B3}'-\mathrm{B2}') + (\mathrm{B3\text{-}B2}) * (\mathrm{B4}'-\mathrm{B1}')]/(\mathrm{B4}'-\mathrm{B1}')(\mathrm{B3}'-\mathrm{B2}')$$

where LSeI is the Liquefaction Sensitivity Index, B1, B2, B3 and B4 are bands corresponding to wavelengths 0.52–0.59 μm, 0.62–0.68 μm, 0.77–0.86 μm, 1.55–1.70 μm of pre-event LISS-III data.
B1′, B2′, B3′, B4′ are that of post-event data of the same wavelength.

Table 1. Attempted band ratios for detecting the soil moisture change

Sr. no.	LSeI	Sensitivity
1	B4 – B1/B4′ – B1′	Medium
2	B4 – B2/B4′ – B2′	Poor
3	(B4′ * B1) – (B4 * B1′)/B1 * B1′	Medium
4	(B4′ * B2) – (B4 * B2′)/B2 * B2′	Poor
5	(B4′ * B3) – (B4 * B3′)/B3 * B3′	Poor
6	(B3′ * B1) – (B3 * B1′)/B1 * B1′	Poor
7	(B4 – B1) * (B3′ – B2′) + (B3 – B2) * (B4′ – B1′)/ (B4′ – B1′) * (B3′ – B2′)	High
8	(B4 – B1) * (B3′ – B2′) – (B3 – B2) * (B4′ – B1′)/ (B4′ – B1′) * (B3′ – B2′)	Medium
9	(B4 – B3)/B1 * B1′/(B4′ – B3′)	Medium

In the case of WiFS sensor, the bands B1 and B4 are absent. Hence, the index abbreviates to:

$$\text{LSeI} = 1 + ((\text{B3} - \text{B2})/(\text{B3}' - \text{B2}'))$$

Thus, the LSeI map derived (Figure 3) shows distinct feature classes. High absorption in NIR and SWIR regions of the post-event data yields very low values depending on

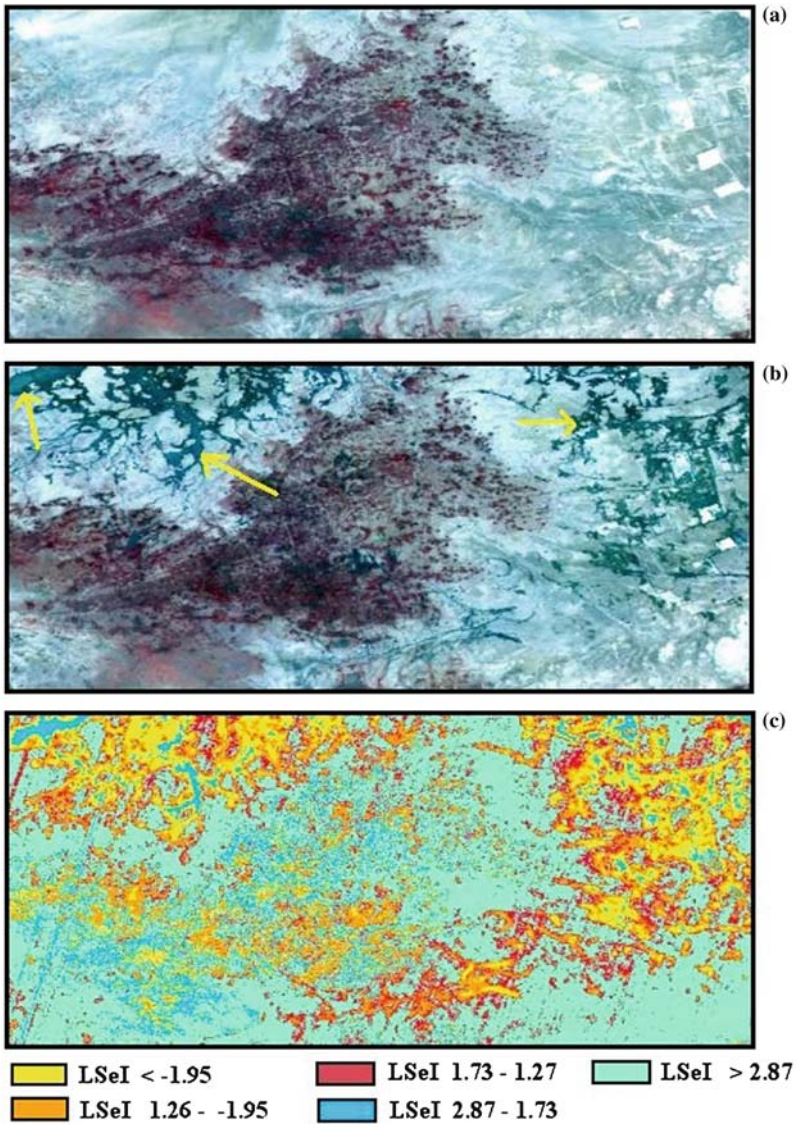

Figure 3. Surface manifestations of Bhuj earthquake 2001 near the epicenter region. (a) Pre-event image. (b) Post-event image. The arrow marks indicate surface water surge due liquefaction. (c) LSI map.

the degree of absorption. Further, the degree of absorption is directly proportional to the amount of moisture.

4.2. TIME-SERIES ANALYSIS USING WIFS DATA

WiFS data sets comprising the immediate pre-event (23rd January, 2001) and post-event (26th and 29th January, 1st and 4th February 2001) are used to study the dynamic changes in soil moisture regime over a period of time. The derived LSeI map is divided into change (LSeI <2.10) and no change (LSeI >2.10) classes on the basis of histogram distribution. The LSeI map derived using the 26th data (Figure 4a) indicate that the Holocene deposits (Younger alluviums, terrace deposits, alluvial fan and colluviums) show sudden increase in soil moisture. Where as on the subsequent days (29th January, 1st and 4th February 2001), soil moisture changes are seen in older alluviums and poorly consolidated Tertiary sedimentary sequences (Figure 4b–d). On account of the very coarse spatial resolution of WiFS data (188 m), the LSeI values are not compared with LSI. However, this LSeI map help in distinguishing the areas with abnormal increase in soil moisture. These identified areas are taken for detailed investigation.

4.3. EVALUATION OF LIQUEFACTION SUSCEPTIBILITY

In order to arrive at a meaningful interpretation, LSeI needs to be validated against the field-based information on liquefaction susceptibility. For this, LSeI map generated at 1:12,000 scale for a small area of 10 km^2 between Bhuj city and airport area is considered for detailed analysis. The LSeI values are compared with the limited test results on liquefaction susceptible criteria such as CRR, CSR and liquefaction severity (LSI) evaluated by following the methods of Youd and Perkins (1987) and Youd et al. (2001).

4.3.1. *Liquefaction susceptibility and lithological setup*

Most part of the investigated area (Bhuj) comprises of Quaternary sediments (Younger and Older alluvium, terrace deposits, alluvial fan) and different types of sandstone of Tertiary and Jurassic periods (Figure 5). The northern parts of the Bhuj city (airport and surrounding area) comprise the Younger, Older alluviums and terrace deposits. From the borehole records (Table 2) it is apparent that the unconsolidated sediments are predominantly sand with several intercalated layers of clay and loam. The thickness of these deposits varies from 2 to 10 m. Occasionally, they exceed 20 m. Lateral extent of these unconsolidated sediments is often restricted to less than a kilometer. Besides these litho types, occasional exposures of shale, basaltic flows and basic dykes are also exposed. On the basis of geology, two liquefaction susceptibility classes are evolved:

Susceptible: Includes unconsolidated Younger alluviums, flood plain deposits, palaeo-channels, alluvial fans and the bajada/colluvial materials with effluent conditions.

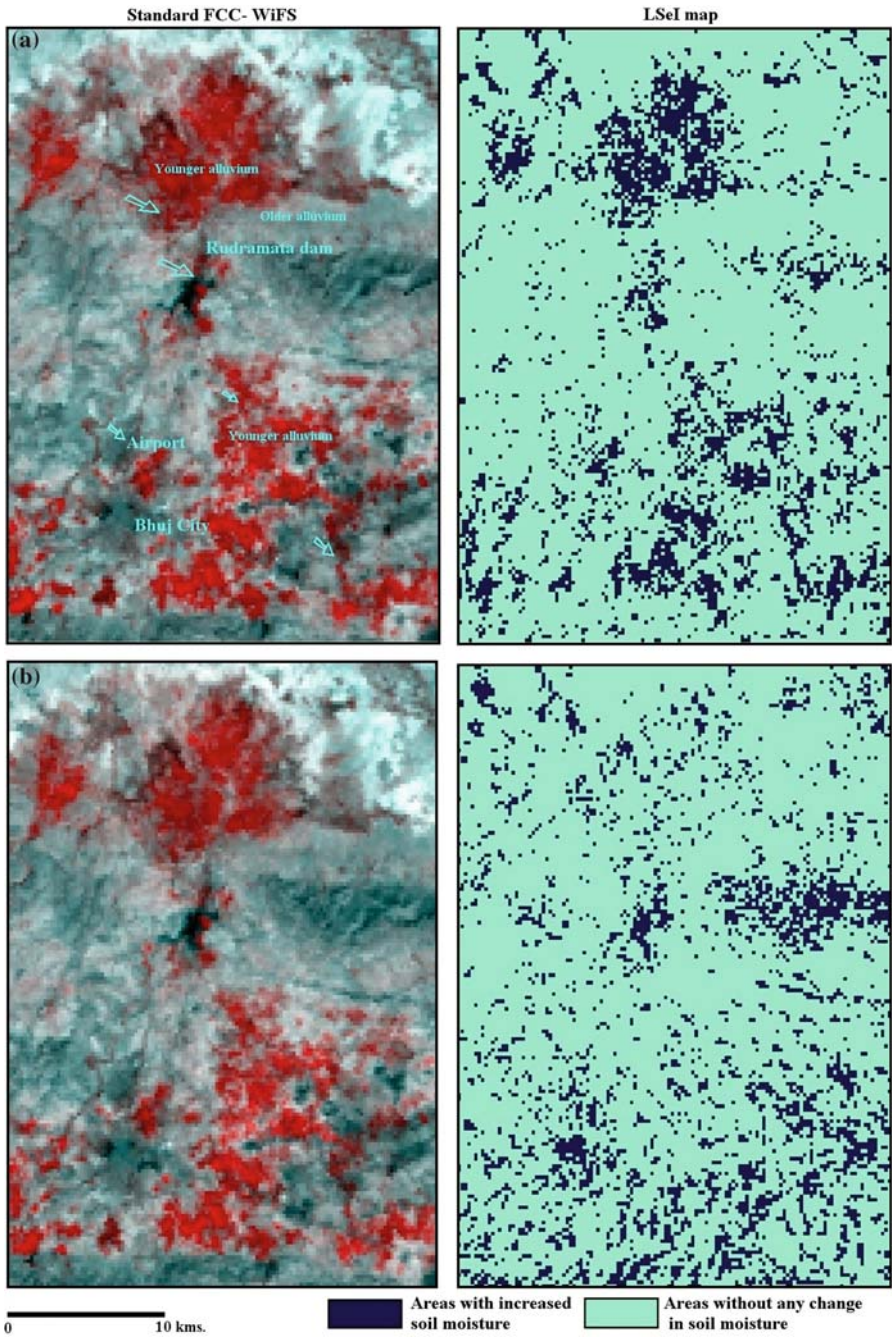

Figure 4. False colour composite (FCC) and LSeI map derived from WiFS data depicting the post-event changes in soil moisture of Quaternary deposits. (a) Image acquired on 26th January 2001. Arrow marks in the FCC indicate the sites where liquefaction was observed in the field. (b) Soil moisture change as on 29th January, 2001 (c) Soil moisture change as on 1st February, 2001 (d) Soil moisture change as on 4th February, 2001.

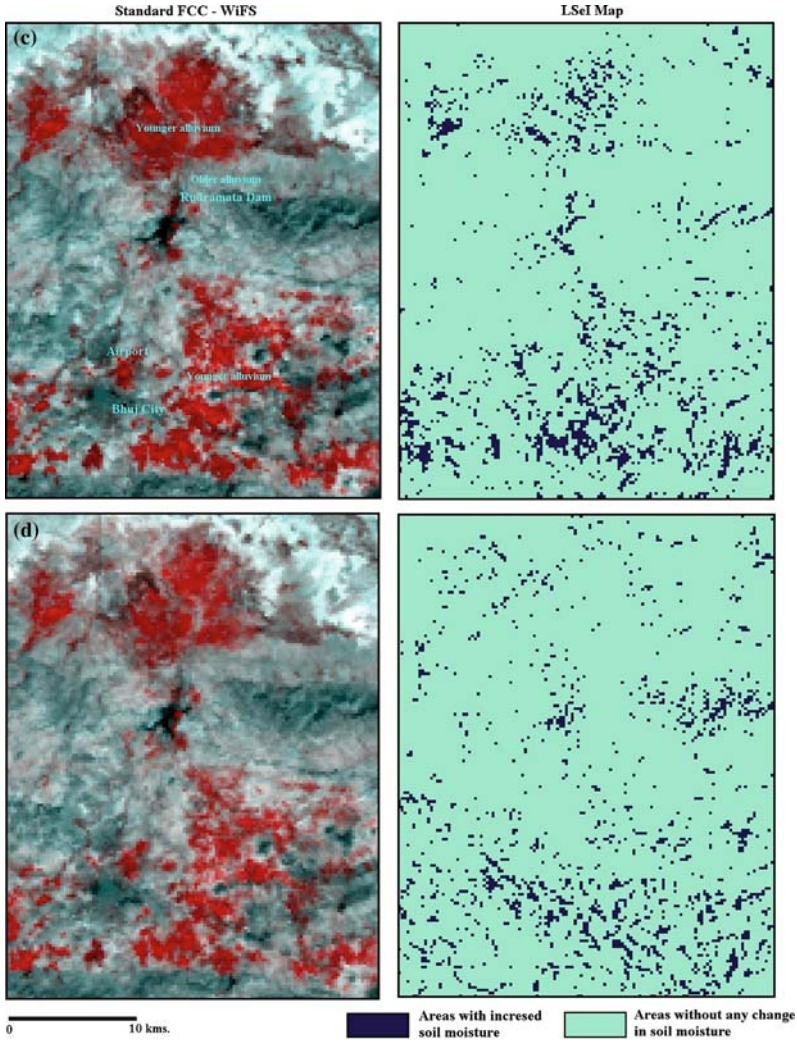

Figure 4. Continued.

Marginally Susceptible: Includes the Older alluvium.
Not Susceptible: Includes the consolidated sedimentary sequences.

4.3.2. *Liquefaction susceptibility and geotechnical criteria*

Evaluation of liquefaction susceptibility requires estimation of seismic demand on a soil layer (generally expressed in terms of CSR) and capacity of the soil to resist liquefaction (expressed in terms of CRR). Standard Penetration Test (SPT) values are widely accepted as a robust technique in evaluating the resistance of soil to liquefaction.

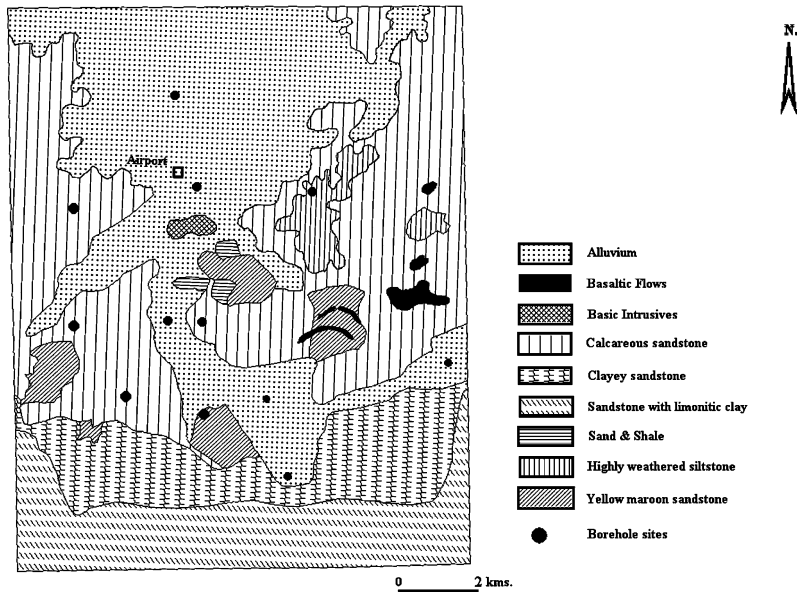

Figure 5. Lithological setup of study area.

In this study, 13 shallow bore holes are made in and around the investigated area and data pertaining to litholog, penetration resistance (SPT), fines content and *in situ* density of the materials are generated (Table 2). The field SPT blow counts are normalized to over burden pressure of 100 kPa and hammer efficiency of 60% $(N_1)_{60}$ by using the following equation:

$$(N_1)_{60} = N_M * C_N * C_E * C_B * C_R * C_S$$

where N_M is the field measured penetration resistance, C_N is $(Pa/\sigma'_{vo})^{0.5}$, the factor to normalize over burden pressure, C_E the correction factor for hammer energy (0.90), C_B the correction for borehole diameter, C_R the correction for rod length and C_S is the correction for sampler. Since the percentage of fines, F(<0.075 mm), also influence the penetration, resistance $(N_1)_{60}$ is further corrected for the influence of fines to equivalent clean sand values $(N_1)_{60cs}$ using the following equation:

$$(N_1)_{60cs} = \alpha + \beta(N_1)_{60}$$

The coefficients α, β are estimated from the following relation:

$$\alpha = 0 \quad \text{for } F \leq 5 \qquad \beta = 1.0 \quad \text{for } F \leq 5$$
$$\alpha = \exp[1.76 - (190/F^2)] \quad \text{for } 5 < F < 35 \qquad \beta = [0.99 + (F^{1.5}/1,000)] \quad \text{for } 5 < F < 35$$
$$\alpha = 5 \quad \text{for } F \geq 5 \qquad \beta = 1.2 \quad \text{for } F \geq 5$$

The CRR and SPT correlation chart adjusted to magnitude of Bhuj earthquake (Mw = 7.7) by Krinitzsky and Hynes (2002) is used herein (Figure 6). Overall index properties of the alluvium include 80–85% sand and 15–20% non-plastic fines.

Table 2. Borehole litholog and basic geotechnical properties of unconsolidated sediments of the study area

Bore hole no.	Location	Depth (m)	Lithology	Fines (%)	D_{50}(mm)	Soil class	SPT ($N_{1,60)cs}$	Density (%)	Depth to water table (m)
BH1	Madhapar	<1	Silty sand	12	0.27	SP-SM	14	40	18.0
		1–5	Coarse sand with pebbles	5	0.56	SP	16	35	
		5–7	Silty sand with clay	20	0.13	SM	28	65	
BH2	North of Bhuj Town	<1	Loamy sand	19	0.14	SM	17	30	17.4
		1–2	Weathered S.St.	NA	NA	NA	49	95	
		2.5	Weathered S.St.	NA	NA	NA	NA	NA	
BH3	East of Bhuj Town	<1	Silty sand & Coarse sand.	6	0.30	SM	11	33	22.5
		1–3	Coarse sand	3	0.40	SP	12	37	
		3–5	Medium-fine sand	11	0.22	SP	25	60	
BH4	Mundra road	<1	Coarse sand	8	0.25	SP-SM	10	36	23.6
		1–2	Weathered S.St.	NA	NA	NA	41	80	
BH5	Airport	<1	Coarse sand with clay	14	0.22	SP-SC	13	25	12.0
		1–2	Sand with clay	11	0.27	SP	33	65	
		2–7	Coarse sand	6	0.42	SP	39	60	
BH6	Rawal Wadi	<2	Silty sand	7	0.21	SM	16	42	19.4
		2–4	Coarse sand	4	1.41	SP	7	23	
		4–8	Coarse sand with clays	20	0.21	SP-SC	50	87	
BH7	Haripar	<1	Coarse sand with silt	8	0.44	SP	15	56	30.0
		1–3	Fine sand with silt	5	0.21	SM	21	37	
		3–5	Coarse sand with clay	11	0.26	SP	31	68	
BH8	Mirzapur	<1	Silty sand	12	0.26	SM	29	35	22.5
		1–2	Coarse sand	5	0.32	SP	7	40	
		2–6	Silty sand	11	0.21	SP-SM	13	48	
		6–9	Weathered S.St.	NA	NA	NA	49	89	

BH9	Near Bhuj cantonment	<1	Silty sand	14	0.27	SM	25	46	25.0
		1–2	Coarse sand with silt	7	0.33	SP	24	68	
		2–3	Weathered S.St.	NA	NA	NA	39	84	
BH10	Ghenla	<1	Coarse sand with clay	21	0.13	SP-SC	11	32	13.2
		1–2	Fine sand with silt, gravel	15	1.12	SP	16	47	
		2–6	Coarse sand	11	0.37	SP	30	55	
		6–7	Weathered S.St.	NA	NA	NA	36	85	
BH11	Sukhapar road	<1	Coarse sand	NA	NA	NA	24	35	20.5
		1–2	Weathered S.St.	NA	NA	NA	46	83	
BH12	Parishram tower	<1	Coarse sand	6	0.42	SP-SM	16	35	8.2
		1–3	Silty sand	13	0.37	SM	28	65	
		3–5	Sand	16	0.24	SP	48	89	
		> 5	Weathered S.St.	NA	NA	NA	NA	NA	
BH13	Airport road	<1	Coarse sand with clay	12	0.19	SP-SC	12	30	21.0
		1–3	Silty sand	9	0.37	SM	26	57	
		3–4	Sand with clays	15	0.22	SP	24	40	
		4–9	Clayey sand	20	0.15	SC	19	67	

S.St. – sandstone; NA – not available.

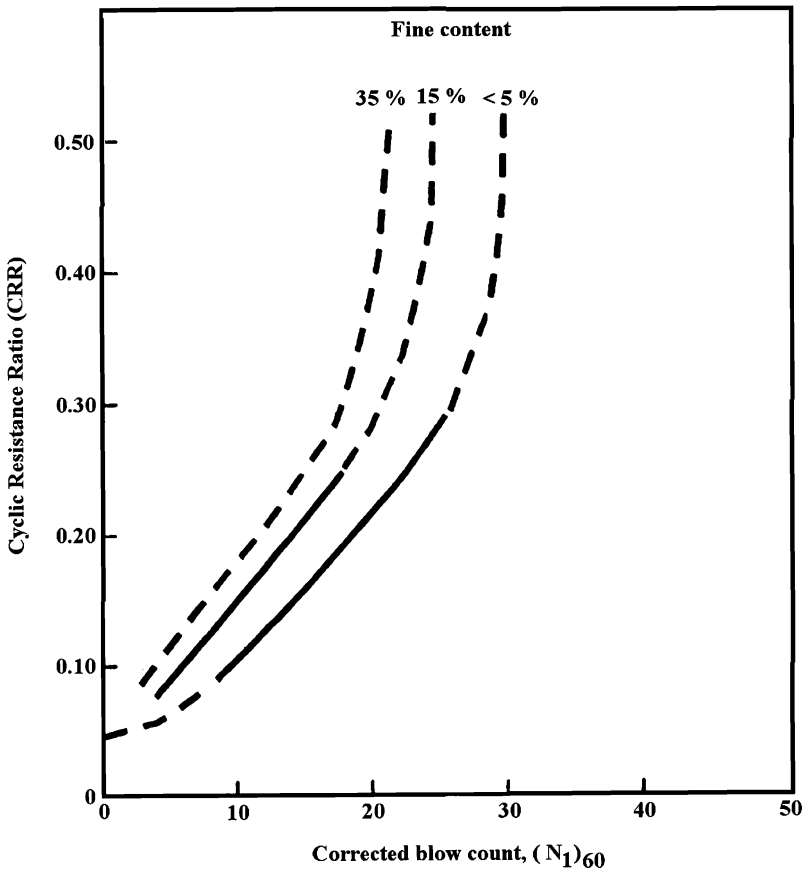

Figure 6. SPT-CRR curves for Mw = 7.7 earthquakes affecting foundation soils. (After Krinitzsky and Hynes, 2002).

The earthquake load measured through CSR is obtained from the simplified equation of Seed and Idriss (1981):

$$\mathrm{CSR} = (\tau_{\mathrm{av}}/\sigma'_{\mathrm{vo}}) = 0.65(a_{\max}/g)(\sigma_{\mathrm{vo}}/\sigma'_{\mathrm{vo}})r_{\mathrm{d}}$$

where $a_{\max}$ is the peak horizontal acceleration at ground surface, g the acceleration due to gravity, $\sigma_{\mathrm{vo}}\sigma'_{\mathrm{vo}}$ the total and effective over burden stress, respectively and r_{d} is stress reduction coefficient estimated from $r_{\mathrm{d}} = 1.0 - 0.00765\,Z$ for depth (Z) $\leqslant$ 9.15 m.

Iyengar and Raghukanth (2002) found that the Bhuj area (which is 65 km away from the epicenter) experienced a Peak Ground Acceleration (PGA) of 0.36–0.38 g. Since the area investigated is less than 10 km^2, a constant PGA value of 0.38 is used.

It is apparent from the CSR, CRR values (Table 3) that the Holocene sediments of the investigated area can undergo liquefaction for the given PGA (0.38 g), magnitude (Mw = 7.7) and epicenter distance (65 km). Again these results are in agreement with filed observation on LSI. On the basis of these geotechnical parameters, the area is classified into three liquefaction susceptible classes viz.

Table 3. Liquefaction susceptibility criteria and observed liquefaction severity of the study area

BH No.	CRR	CSR	Liquefaction susceptibility	Observed LSI	LSeI
BH1	0.22	0.25	Yes	20	0.380
BH2	0.25	0.23	Marginal	5	2.277
BH3	0.38	0.26	No	2	2.706
BH5	0.22	0.23	Yes	10	1.600
BH6	0.22	0.23	Yes	10	1.600
BH7	0.32	0.25	No	5	2.312
BH8	0.34	0.26	No	–	3.015
BH9	0.27	0.24	Marginal	–	3.521
BH10	0.33	0.25	No	2	2.606
BH12	0.22	0.25	Yes	7	2.428
BH13	0.21	0.23	Yes	20	0.351

Susceptible: Includes unconsolidated sediments with CRR $\leqslant$ CSR).
Marginally susceptible: Includes unconsolidated sediments with CRR slightly higher than CSR).
Not susceptible: Includes unconsolidated sediments and weakly consolidated sediments with CRR > CSR).

4.3.3. *Liquefaction susceptibility and hydrogeology*

Saturation being important criteria, depth to reduced water level is obtained in and around Bhuj and contours are constructed based on the data collected from 40 wells for December 2000 (Table 2). The depth to water table varies from 8.2 to 30 m. The alluvium comprises several shallow and perched aquifers. Hence, the alluvial areas with perched aquifers and shallow water table enhance the scope of saturation and liquefaction. From the water table contours, three classes of liquefaction susceptibility are derived:

- *Susceptible*: Younger alluvium and terrace deposits with depth to water table <10 m.
- *Marginally susceptible*: Younger and Older alluvium with depth to water table 10–15 m.
- *Not susceptible*: All the litho units with depth to water table >15 m.

4.4. LSeI AND LSI RELATION

In evaluating the LP, LSI is (Youd and Perkins, 1987) widely used as a measure of liquefaction severity. In this study, attempt is made to compare the LSeI with the field-based observations on LSI. In all, thirty field based ground failure observations (with GPS co-ordinates) are resolved into their corresponding LSI values (Table 4). These values range from 2 to as high as 60 in Bhuj and surrounding areas. In the investigated area, the LSI values vary from 2 to 20. The derived LSeI values range

Table 4. List of sampling sites depicting the relationship between LSI and LSeI

Sr. No.	Location	Type of ground failure	LSI	LSeI
1	Khavda-I	Sand blows, craters	50	–2.01
2	Khavda-II	Sand blows, craters	30	–1.35
3	Khavda-III	Sand blows, craters, fissures	50	–1.95
4	Bhirandiala-I	Lateral spreads, craters	50	–1.98
5	Bhirandiala-II	Lateral spreads, craters	30	–1.52
6	Banni-I	Craters, sand blows	50	–2.14
7	Banni-II	Craters, sand blows	50	–1.86
8	Kunaria	Fissures, craters	10	+1.55
9	Nirona	Lateral spreads, sand blows	02	+2.10
10	Bhuj (Airport area)	Lateral spreads, sand blows, craters	10–20	+1.62
11	W. Dhrang	Lateral spreads, fissures	10	+1.51
12	E. Dhrang	Lateral spreads, craters	02	+1.99
13	Lakharia Wandh	Lateral spreads, craters, sand blows	07	+1.72
14	Budharmora	Lateral spreads, craters, sand blows	30	+0.95
15	Madhpar	Lateral spreads, craters, sand blows	15	+1.84
16	Khadir	Sand blows	50	–1.96
17	Lodai	Craters, sand blows	50–60	–2.17
18	Chobari-I	Fissures, sand blows	40	–1.71
19	Rudramata	Fissures, lateral spreads	10–20	+1.32
20	Manfara	Fissures, slumps,	10–30	+1.30
21	Kotada	Lateral spreads, craters	05	+1.88
22	Anjar	Fissures, craters	05–10	+2.09
23	Chobari-II	Lateral spreads, craters, fissures	30	+0.69
24	Bhurudia	Lateral spreads, fissures	50	–2.04
25	Khengarpar	Lateral spreads, craters, fissures	30–50	–1.81
26	Wondh	Lateral spreads, craters, sand blows	30–50	–1.11
27	Little Rann	Craters, sand blows	30–50	–1.96
28	Chadawala	Fissures, craters	05–10	+1.74
29	Samkhiali	Fissures, craters	10–30	+1.28
30	Ratnal	Fissures, craters	10–30	+1.61
31	Mundra	Lateral spreads, fissures	10	+1.74

from −2.23 to +2.12 for liquefied areas. The areas severely affected by liquefaction (LSI >40) exhibit negative LSeI values due to strong absorption in NIR and SWIR bands. Where as, the un-liquefied areas generally show positive LSeI values (>2.78). The scatter plots (Figure 7) of LSI and LSeI show strong correlation ($R^2 = 0.97$). The best fit second-order polynomial equation with an RMS error of 0.30 is given as

$$\mathrm{LSI} = 0.852\mathrm{LSeI}^2 - 10.301\mathrm{LSeI} + 24.076$$

This relationship helps in classifying the LSeI image into five categories (Figure 8) on the basis of LSI values.

Very high (LSI: >40; LSeI: <–1.95)
High (LSI: 20–40; LSeI : 1.26–1.95)
Medium (LSI: 5–20; LSeI: 1.73–1.27)

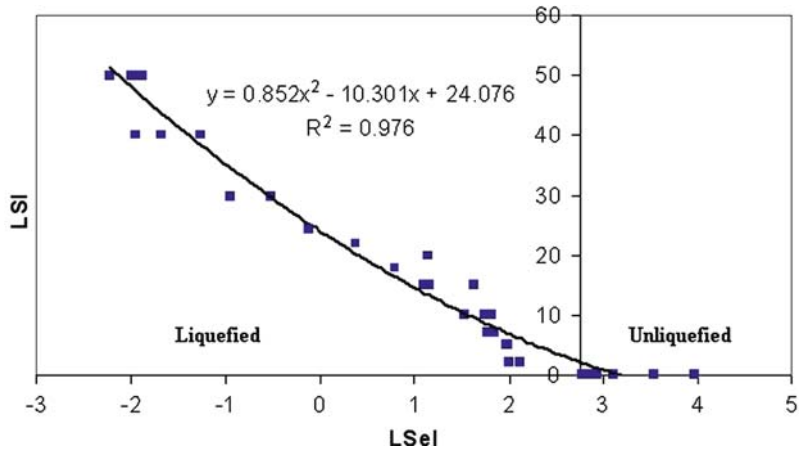

Figure 7. LSI–LSeI correlations for the Bhuj earthquake 2001.

Low (LSI: <5; LSeI: 2.78−1.74)
Unliquified (LSeI: >2.78)

5. Discussion and Conclusions

This study mainly focuses on identifying the areas in and around Bhuj with abnormal increase in soil moisture after the Bhuj earthquake in 2001. The basic principle behind using the satellite images in mapping the soil moisture changes is that water absorbs energy in the NIR and SWIR regions of electromagnetic spectrum. Attempted band ratio (LSeI) among the pre- and post-SWIR, NIR, red and green bands help to distinguish reflectance of soils by its moisture content.

The LSeI derived from WiFS data that was procured immediately after the earthquake indicate that there is more absorption in NIR band in Younger alluvium, and terrace deposits (Figure 4a). The sudden decrease in reflectance of theses units indicates an increase in soil moisture content. Similar increase in soil moisture is observed in Older alluvium and some parts of Younger alluvium on subsequent days (Figure 4c, d). This delayed observation in soil moisture increase is attributed to:

(1) post-quake tremors with magnitudes measuring up to six;
(2) liquefaction of a deeper layer;
(3) rise in water table;
(4) delay in mapping due to non availability of satellite passes on 27th, 28th January 2001.

The LSeI map generated from the LISS-III data at 1:12,000 scale clearly indicates (Figure 8) increase in soil moisture in Younger alluvium and Older alluvium. Field observations on liquefaction severity assessed in terms of LSI are of the order of 50–60 near the epicenter. In Bhuj city and its surroundings the LSI varied from 2 to

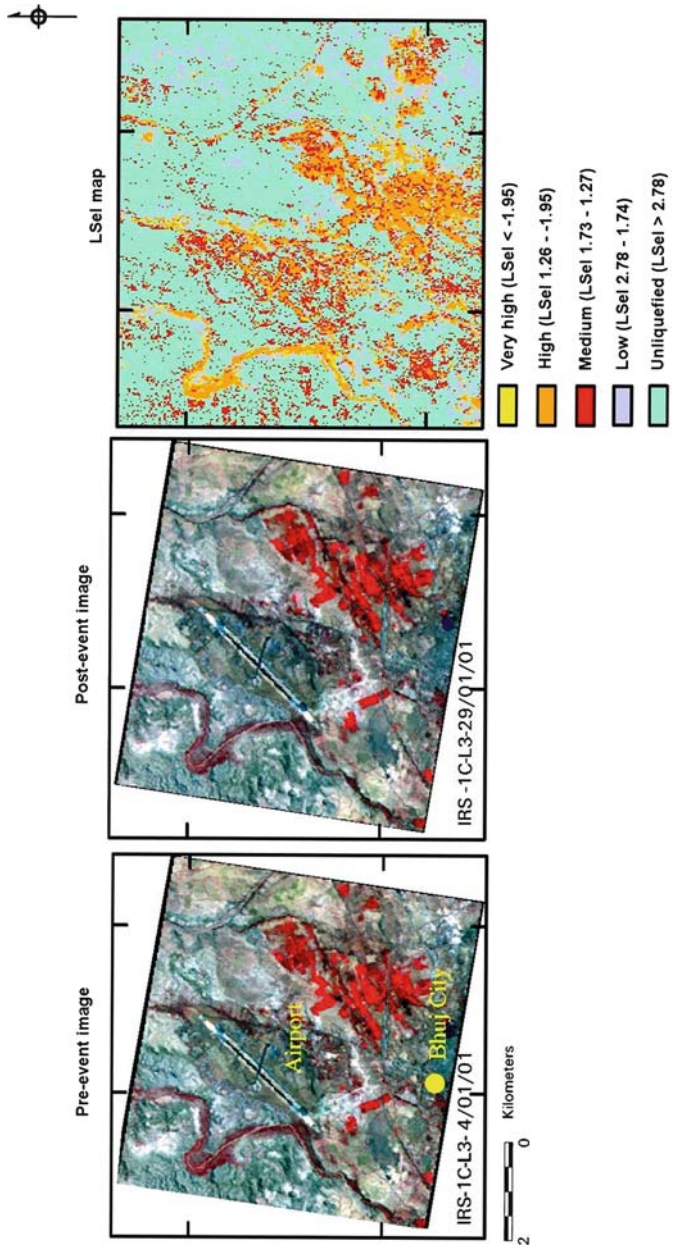

Figure 8. LSeI map of Bhuj Airport area derived from IRS-LISS-III data.

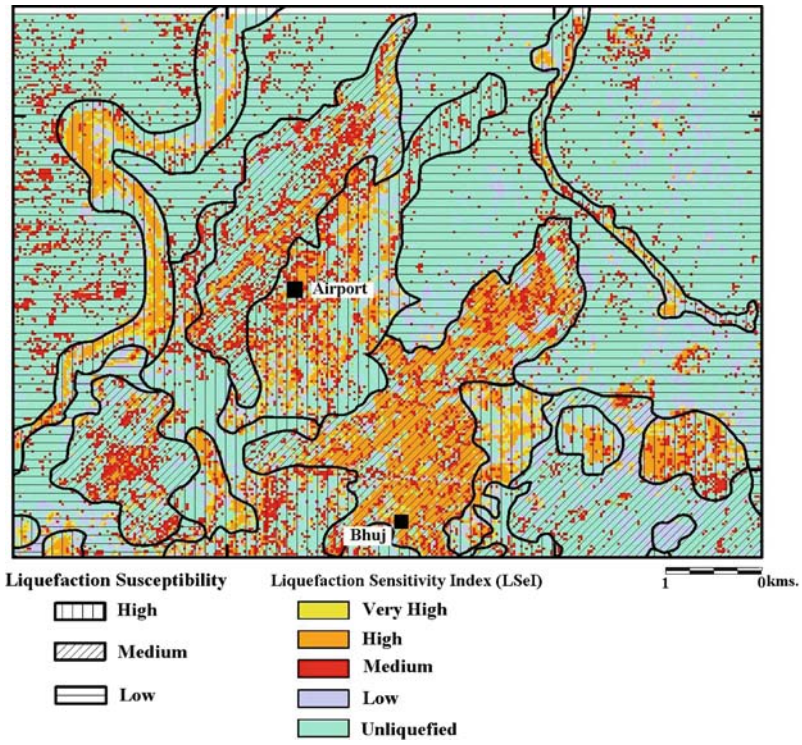

Figrue 9. Overlay of liquefaction susceptibility map and LSeI.

20. The LSeI values derived for the same location vary from –2.2 to +2.3. It is observed that the areas severely affected by liquefaction (LSI >40) gives negative LSeI values. The un-liquefied areas show positive LSeI values (>2.78). The scatter plots made between the observed LSI values and derived LSeI values has very strong correlation ($R^2 = 0.97$). This observation clearly points that satellite derived soil moisture changes are strongly related to liquefaction.

Limited geotechnical studies on SPT, soil density, grain size and derived values on CSR, CRR indicate that in most of the areas the ratio between demand and capacity suffice the requirements for liquefaction. It is evident from the results (Table 3) that the LSeI values match well with the accepted criteria on liquefaction evaluation (Youd et al., 2001).

The spatial database on geology, LSeI, LSI, depth to water table, bore holes and attribute data on litholog, SPT, fine content, CSR and CRR are integrated in GIS (ARC/Info) environment. From this database, contours of SPT, density and depth to water table are generated. From the overlay analysis of LSeI and the liquefaction susceptibility criteria, a liquefaction susceptibility map (Figure 9) is prepared for the Bhuj area considering the following criteria:

High susceptible area: Areas with unconsolidated sediments (Younger alluvium) having CRR $\leqslant$ CSR, low LSeI values < 1.26, LSI values ≥ 20 and depth to water table less than 10 m.

Moderately susceptible: This include areas with *unconsolidated* sediments (Younger alluvium) having CRR values slightly more than CSR, LSeI values 1.73–1.27, LSI values 10–20 and depth to water table less than 10–15 m.

Low susceptible: This include areas with *unconsolidated* and *poorly consolidated* sediments (Older alluvium) having CRR slightly more than CSR, LSeI values 1.74–2.78, LSI values < 10 and depth to water table 10–15 m.

Not susceptible: This include areas with *unconsolidated* and *poorly consolidated* sediments (Older alluvium) having CRR values more than CSR, LSeI values > 2.78 and depth to water table > 15 m.

It can be concluded that, the derived LSeI classes match well with field-based observation on liquefaction susceptibility (CRR, CSR) and liquefaction severity (LSI). Thus, the LSeI offers quick and efficient tool in mapping the post-event liquefaction occurrence (Ramakrishnan et al., 2003). However, LSeI cannot be used to predict the LP. Since liquefaction susceptibility mapping of earthquake prone Kachchh area is still in its infancy, this methodology could be of use in evaluating the liquefaction susceptibility of this area.

Acknowledgements

The Authors are thankful to ISRO, Department of Space for funding this research project. First author is thankful to Dr. K.C. Tiwari and Dr. Parag Sohani, Department of Geology, M.S. University of Baroda and Mr. Y. Jadeja, Abhiyan foundation, Bhuj for their help in technical discussion and data collection. Technical comments from Dr. Jose Delgado, Alicante, Spain is highly helpful in improving the quality of the paper. Authors are thankful to the reviewers for their comments.

References

Bilham, R. (2001) 26th January Bhuj earthquake, Gujarat, India http://www.cirec.colorado.edu/~bilham/Gujarat2001.html.

Biswas, S.K. and Khattri, K.N. (2002) Geologic study of earthquake in Kutch, Gujarat, India, *Journal of the Geological Society India*, **60**(2), 131–142.

Carper, W.J., Kiefer, R.W and Lilesand, T.M. (1990) The use of intensity – hue-saturation transformation's for merging SPOT Panchromatic and multispectral image data, *Photogrammetric Engineering and Remote Sensing*, **56**(4), 459–467.

Gupta, R.P., Saraf, A.K. and Chander, R. (1998) Discrimination of areas susceptible to earthquake induced liquefaction from landsat data, *International Journal of Remote Sensing*, **19**, 569–572.

Iyengar, R.N. and Raghukanth, S.T.G. (2002) Strong Ground motion at Bhuj city during the Kutch Earthquake, *Current Science*, **82**(11), 1366–1372.

Jade, S., Mukul, M., Parvez, I.A., Ananda, M.B., Kumar, P.D. and Gaur, V.K. (2001) Estimates of Coseismic displacement and post-seismic deformation using GPS geodesy for the Bhuj earthquake of 26th January 2001, *Current Science*, **82**(6), 748–752.

Karanth, R.V., Sohoni, S.P., Mathew, G. and Khadkikar, A. (2001) Geological observations of the Bhuj earthquake, *Journal of the Geological Society of India*, **58**, 193–202.

Krinitzsky, E.L. and Hynes, M.E. (2002) The Bhuj, India earthquake: lessons learnt for earthquake safety of dams on alluvium, *Engineering Geology*, **66**(3–4), 163–196.

Malik, J.N., Sohoni, P.S., Karanth, R.V. and Merh, S.S. (1999) Modern and historic seismicity of Kachchh Peninsula, Western India, *Journal of the Geological Society of India*, **54**, 545–550.

McFetters, S.K. (1996) The use of normalized difference water index (NDWI) in the delineation of open water features, *International Journal of Remote Sensing*, **17**(7), 1425–1432.

Mohanty, K.K., Maiti, K. and Nayak, S. (2001) Monitoring water surges, *GIS Development*, **3**, 32–33.

Oldham, R.D. (1926) The Kutch earthquake of 16th June 1891 with revision of the great earthquake of 12th June 1897, *Memoirs of the Geological Survey of India*, **46**, 47–71.

Rajendran, K., Rajendran, C.P., Thakkar, M. and Tuttle, M.P. (2001) The 2001 Kutch (Bhuj) earthquake: coseismic surface features and their significance, *Current Science*, **80**(11), 1397–1405.

Ramakrishnan, D., Jeyaram, A., Mohanty, K.K. and Nayak, S.R. (2003) Mapping the liquefaction susceptible zones in parts of Kachchh region using IRS-WiFS and LISS-III data, in Proceedings of the International Workshop on Earth System Process Related to Gujarat Earthquake Using Space Technology, 27–29 January 2003, Department of Civil Engineering, IIT, Kanpur, India, pp. 50–51.

Ray, C.D.K., Foreste, K. and Roy, P.S. (2001) Detection and analysis of surface changes due to recent earthquake in Gujarat using IRS PAN and LISS-III data, in Proceedings of the Workshop on Recent Earthquake of Chamoli and Bhuj, 22–23 May 2001, Indian Society of Earthquake Technology, Roorkee, India, pp. 225–236.

Saraf, A.K. (2000) IRS IC-PAN depicts Chamoli earthquake induced landslide in Garhwal Himalayas, India, *International Journal of Remote Sensing*, **21**, 2345–2352.

Saraf, A.K., Sinvhal, A., Sinvhal, H., Ghosh, P. and Sarma, B. (2002) Satellite data reveals 26 January 2001 Kutch Earthquake-induced ground changes and appearance of water bodies, *International Journal of Remote Sensing*, **23**(9), 1749–1756.

Seed, H.B. and Idriss, I.M. (1981) Evaluation of liquefaction potential of sand deposits based on observations of performance in previous earthquakes, in Proceedings of the ASCE National Fall Convention, St. Louis, Session, January, Vol. 24.

Sharma, J.R., Gupta, A.K., Sreenivasan, G. and Bhadra, B.K. (2003) Damage Assessment of Bhuj earthquake (2001) using IRS LISS-III and PAN data, in Proceedings of the International Workshop on Earth System Process Related to Gujarat Earthquake Using Space Technology, 27–29 January 2003, Department of civil engineering, IIT Kanpur, India.

Singh, R.P., Bhoi, S., Sahoo, A.K., Raj, U. and Ravindranath, S. (2001) Surface Manifestations after the Gujarat Earthquake, *Current Science*, **81**(2), 164–166.

Sohani, P.S. (2002) Tectono – Structural attributes of Central Kachchh Mainland with special emphasis on active tectonics and Palaeoseismicity, *Journal of the Geological Society of India*, **60**, 114–116.

Townshed, J.R.G. and Justice, C.O. (1986) Analysis of the dynamics of African vegetation using Normalized Vegetation Index, *International Journal of Remote Sensing*, **7**, 1435–1445.

Tucker, C.J. and Sellers, P.J. (1986) Satellite remote sensing of primary productivity, *International Journal of Remote Sensing*, **7**, 1395–1416.

Tuttle, M.P. and Hengesh, J.V. (2002) Liquefaction, in Bhuj, India Earthquake of January 26, 2001 Reconnaissance Report (edited by Jain, S.K, Lettis, W.L, Murty, C.V.R and Barder, J.P). Earthquake Spectra, **18**(Suppl.), 79–100.

Youd, T.L. and Keefer, D.K. (1981) Earthquake induced ground failures, in Facing geologic and hydrologic hazards, U.S. Geological Survey Professional Paper 1240-B, pp. 23–31.

Youd, T.L. and Perkins, D.M. (1987) Mapping of Liquefaction Severity Index, *Journal of Geotechnical Engineering, ASCE*, **113**(11), 1374–1392.

Youd, T.L., Idriss, I.M., Andrus, R.D., Arango, I, Castro, G, Christian, J.T., Dobry, R., LiamFinn, W.D., Harder, L.F. Jr, Hynes, M.E., Ishihara, K., Koester, J.P., Laio, S.S.C., Marcuson, W.F. III, Martin, G.R., Mitchell, J.K., Moriwaki, Y., Power, M.S., Robertson, P.K., Seed, R.B. and Stokoe, K.H. II (2001) Liquefaction resistance of soils: summary report from the 1996 NCEER and 1998 NCEER/NSF workshops on evaluation of liquefaction resistance of soils, *Journal of Geotechnical and Geoenvironmental Engineering*, **127**(10), 817–833.

Wang, C., Qi, J., Moran, S. and Marsett, R. (2004) Soil moisture estimation in semi arid rangeland using ERS-2 and TM imagery, *Remote Sensing of Environment*, **90**, 178–189.